ORGANIC PROCESS RESEARCH & DEVELOPMENT
OPR&D

pubs.acs.org/OPRD

Article

Deracemization via Periodic and Non-periodic Temperature Cycles: Rationalization and Experimental Validation of a Simplified Process Design Approach

Francesca Breveglieri, Brigitta Bodák, and Marco Mazzotti*

Cite This: *Org. Process Res. Dev.* 2021, 25, 2551−2565

Read Online

ACCESS | Metrics & More | Article Recommendations

ABSTRACT: Solid-state deracemization via temperature cycles is a promising technique that combines crystallization and racemization in the same batch process to attain enantiomer purification. This method is particularly attractive because the target enantiomer can be isolated with a 100% yield, and a large number of operating parameters can be adjusted to do this effectively. However, this implies that several choices need to be made to design the process for a new compound. In this work, we provide a solution to this dilemma by suggesting a simplified model-free design approach based on a single dimensionless parameter, that is, the dissolution factor, that represents the cycle capacity. This quantity is obtained from a novel rescaling of the model equations proposed in previous work and acts as a handy design parameter because it only depends on the operating conditions, such as the suspension density, the enantiomeric excess, and the difference in solubility between high and low temperatures in the cycle. With extensive modeling studies, supported by experimental results, we demonstrate the primary and general effect of the dissolution factor on the deracemization process and thus its relevance for the process design. Through both experiments and simulations, we rationalize and evaluate the process performance when periodic and non-periodic temperature cycles are applied to the deracemization of virtual and real compounds with different properties, that is, growth rate and solubility. Based on the approach proposed here, we clarify how the combined effect of more operating conditions can be exploited to obtain quasi-optimal process performance, which results superior when deracemization via periodic temperature cycles is performed.

KEYWORDS: *deracemization, temperature cycles, process design, effect of kinetics, compound-specific behavior*

1. INTRODUCTION

Enantiomers are well known for exhibiting identical physical and chemical properties in symmetric environments but for being different under chiral conditions.[1] This feature is particularly relevant for pharmaceutical applications, which require isolating the pure target enantiomer (eutomer) to avoid the effects caused by the undesired species (distomer).[2,3] To address this challenging separation task, several processes have been developed.[4] Among them, crystallization-based methods, such as preferential crystallization[5] and solid-state deracemization,[6−10] are preferred since they enable to collect a highly pure product in its solid form. Particularly, deracemization processes have the advantage of transforming the undesired enantiomer of a racemizable conglomerate-forming compound into the desired one, thus increasing the process yield. This conversion occurs when a suspension of enantiomerically enriched solids partially dissolves, so as the distomer racemizes in solution, the eutomer crystals grow, thus enabling the attainment of enantiopurity. The batch implementation of such a process is defined as attrition-enhanced deracemization if particles' dissolution and growth are induced by grinding the solids to form small fragments that can easily dissolve[7,8,10] or deracemization via temperature cycles if the suspension undergoes periodic temperature variations.[6,11] The latter method has been widely studied in the past years because of its easy implementation in a thermostated stirred tank reactor and the availability of numerous operating parameters, which can be adjusted to achieve the target specifications. Different works focused on the effect of such operating conditions on the process performance in order to master the design of highly productive operations.[12−18] Among the parameters investigated, we find notably the initial enantiomeric excess and the temperature range and also the amplitude of the temperature cycle and the initial suspension density, which contribute to determine the amount of solid that can dissolve, and thus potentially deracemize, in each temperature cycle. A few researchers found that the process is faster when a larger fraction of the solid amount is dissolved per temperature cycle.[11,16,19,20] This is expected because in this case, the distomer amount that can convert is larger, but it is also surprising considering that a larger amount of the eutomer can dissolve as well.

In this work, we elaborate on the amount dissolved only with respect to the undesired enantiomer present by

Received: August 2, 2021
Published: November 5, 2021

ACS Publications

© 2021 The Authors. Published by American Chemical Society

https://doi.org/10.1021/acs.oprd.1c00310
Org. Process Res. Dev. 2021, 25, 2551−2565

Table 1. Model Equations in the Dimensional Form[14]

PBEs	$\frac{\partial f_i}{\partial t} + \frac{\partial (G_i f_i)}{\partial L} = 0, \quad i = L, D$ (1)
mass balance equations	$\frac{dc_i}{dt} = -k_v \rho_c \frac{d\phi_{3,i}}{dt} + R_i(c_i, c_j, T), \quad j = D, L$ (2)
constitutive equations	
bulk solubility	$c_{\infty,i}(T) = q_0 \exp\left(-\frac{q_1}{T}\right)$ (3)
size-dependent solubility	$c_i^*(T, L) = c_{\infty,i}(T)\exp\left(\frac{\alpha_0}{LT}\right)$ (4)
growth/dissolution rate	$G_i(S_{\infty,i}, T, L) = A \exp\left(-\frac{B}{RT}\right)\left(S_{\infty,i} - \exp\left(\frac{\alpha_0}{LT}\right)\right)$ (5)
growth	$A = k_{g,0}, B = E_g, S_{\infty i} > 1$
dissolution	$A = k_{d,0}, B = E_d, S_{\infty i} \leq 1$
racemization rate	$R_i(c_i, c_j, T) = k_r(T)(c_j - c_i) = k_{r,0} \exp\left(-\frac{E_r}{RT}\right)(c_j - c_i)$ (6)
nth moment of the PDF f_i	$\phi_{n,i} = \int_0^\infty L^n f_i(L, t) dL$ (7)
initial and boundary conditions	$f_i(L, t = 0) = f_{i,0}(L)$ $f_i(0, t) = 0$ $c(T(t = 0)) = c_\infty(T(t = 0))$ (8)

combining these two pieces of information in a single parameter, that is, the *dissolution factor*, that quantifies the deracemization potential of the cycles. Specifically, the initial value of this quantity is given by the ratio between the initial amount of the undesired enantiomer in the solid phase and the variation of its concentration (at solubility) between the high and low temperatures of the cycle. Because the distomer mass varies during deracemization and the temperature window of operation may change in the case of non-periodic temperature cycles, the dissolution factor can be recalculated at every cycle. Interestingly thus, the dissolution factor can be used both as a design parameter (when considering its initial value) and as a diagnostic parameter (when considering its cycle-by-cycle definition). It is also worth noting that the dissolution factor stems rather naturally from a novel approach of how to normalize the model equations.

First, we rationalize the design of the deracemization of different compounds based on the dissolution factor through simulations and experiments. We analyze the effect of operating conditions and interpret it in terms of the value of this dissolution factor. With the aid of the population balance equation (PBE) model, previously developed in our group and adapted here to the purpose of this work, we examine how the productivity of periodic temperature cycle deracemization processes is enhanced when the dissolution factor is at a particularly low value, that is, when a large distomer amount is dissolved. Based on these results, in the second part of the study, we analyze if and how the deracemization time changes when the period and the amplitude of the temperature cycles are modified over time during the deracemization process. To this aim, we consider once again the evolution of the dissolution factor during the process itself. Such cycles are defined as non-periodic temperature cycles because we vary both the period and amplitude. Considering that this strategy was already proposed in the literature,[21] we rationalize the previous findings through targeted simulations, supported by novel experimental results.

The paper is structured as follows: first, we summarize the mathematical model of periodic and non-periodic temperature cycle processes, focusing on a novel scaling approach, which enables to highlight the important role played by the dissolution factor. Then, we describe the choice of the simulation conditions and how the process performance is assessed. We also present the experimental protocol and conditions. In Section 4, we discuss the simulation and experimental results of the deracemization process when periodic cycles are performed, while the implications of non-periodic temperature profiles are analyzed in Section 5. Finally, we summarize the relevant conclusions of this contribution.

2. THEORY

2.1. Mathematical Model. In this section, we summarize the mathematical model, previously developed in our group for the study of deracemization via temperature cycles.[14] Moreover, we present the rationale behind this work, which is justified by deriving an alternative rescaling of the model equations.

The mathematical model of the deracemization via the temperature cycle process is a population balance equations (PBEs)- based model formulated in terms of rescaled equations derived in detail in Section 3 by Bodák et al.[14] The PBEs are solved with a high-resolution finite volume method[22] (for details on the solution of the equation, see Bodák, in preparation[23]). Table 1 summarizes the dimensional model equations, on which the theoretical part of this study is based. It is worth noting that we assume that neither nucleation nor breakage or agglomeration occurs during deracemization; hence, the right-hand side (rhs) of eq 1 is 0.

These equations clearly show that several operating conditions need to be set to design and operate the deracemization process. As indicated by experimental[11,12,16,24] and modeling studies,[14,25] such a choice can be difficult, particularly when considering different compounds with completely different solubilities, growth rates, etc./enleadert-

https://doi.org/10.1021/acs.oprd.1c00310
Org. Process Res. Dev. 2021, 25, 2551−2565

wodots. We aim at providing tools to rationalize the process design by clarifying the interplay among these operating parameters and the system properties, which are all components of the model parameters. We can achieve this goal by rescaling the model equations in a way that is different from and independent of how they are treated and solved numerically here and in previous works.[14]

To this aim, let us introduce the following dimensionless quantities:

$$\lambda = \frac{L}{L_r}, \qquad \tau = \frac{t}{t_r}, \qquad \theta = \frac{T}{T_r} \tag{9}$$

$$\hat{f}_i(\lambda) = L_r f_i(L) \tag{10}$$

$$\hat{\phi}_{3,i} = \frac{\phi_{3,i}}{\phi_r} \tag{11}$$

$$\hat{c}_i = \frac{c_i}{c_r} \tag{12}$$

$$\widehat{G}_i = \frac{t_r}{L_r} G_i \tag{13}$$

The five scaling factors, that is, L_r, t_r, T_r, ϕ_r, and c_r, can be purposefully selected so as to reduce the model equations to a simple and useful form, where the model parameters are grouped in a number of dimensionless quantities as small as possible. Thus, the reference time is defined as the inverse of the racemization pre-exponential factor, $t_r = 1/k_{r,0}$, while the reference length is chosen as $L_r = t_r k_{g,0}$ (the reference temperature, T_r, does not play an important role here and can be chosen arbitrarily, e.g., 273 K).

After substituting these dimensionless variables in eqs 1−8, the coefficient of the first term on the rhs of eq 2 equals $(k_v \rho_c \phi_r)/c_r$. Although in principle we could choose ϕ_r and c_r so as to make this group equal 1, in practice, it is insightful to make a choice that allows this term to obtain a physical meaning. Let us note that this group weighs the contribution of the accumulation in the solid phase, that is, $d\phi_3^L/d\tau$, with respect to that in the liquid phase, $dc_L/d\tau$. By letting the reference third moment of the PSD, ϕ_r, be equal to $\phi_{3,0}^L$, that is, the third moment of the initial distomer PSD, and the reference concentration, c_r, be defined as $\Delta c_\infty = c_\infty^L(T_{max}) - c_\infty^L(T_{min})$ (the superscript "L" is then neglected for simplicity), we obtain for the coefficient above, called δ_0, the following expression:

$$\delta_0 = \frac{k_v \rho_c \phi_{3,0}^L}{\Delta c_\infty} = \frac{\rho_0^L}{\Delta c_\infty} = \frac{\rho_0(1 - ee_0)}{2\Delta c_\infty} \tag{14}$$

This is defined as *dissolution factor* and corresponds to the ratio between the initial amount (hold-up) of the undesired enantiomer in the solid phase, which has to be converted into the target enantiomer via dissolution and racemization, and the capacity of the solution, that is, the maximum enantiomer's amount that can potentially dissolve and convert during every cycle, which is given by the difference in nominal solubility (eq 3) between T_{max} and T_{min}, namely, Δc_∞. On one hand, the numerator is proportional to the distomer mass, ρ_0^L, which can also be computed from the total initial suspension density, that is, $\rho_0 = k_v \rho_c (\phi_{3,0}^D + \phi_{3,0}^L)$, and the initial enantiomeric excess, that is, $ee_0 = (\phi_{3,0}^D - \phi_{3,0}^L)/(\phi_{3,0}^D + \phi_{3,0}^L)$ (see the last term in eq 14). On the other hand, by choosing a value for the denominator, the amplitude of the temperature profile, that is, ΔT, for a specific compound with a specific solubility curve is defined (or vice versa).

With this selection of parameters, we obtain the following rescaled PBEs, material balances, and constitutive equations

$$\frac{\partial \hat{f}_i}{\partial \tau} + \frac{\partial(\widehat{G}_i \hat{f}_i)}{\partial \lambda} = 0, \qquad i = L, D \tag{15}$$

$$\frac{d\hat{c}_i}{d\tau} = -\delta_0 \frac{d\hat{\phi}_{3,i}}{d\tau} + \exp\left(-\frac{\theta_r}{\theta}\right)(\hat{c}_j - \hat{c}_i), \qquad j = D, L \tag{16}$$

$$\hat{G}_i = \exp\left(-\frac{\theta_g}{\theta}\right)\left(S_{\infty,i} - \exp\left(\frac{\alpha_\theta}{\lambda\theta}\right)\right) \text{with} \quad S_{\infty,i} = \hat{c}_i/\hat{c}_{\infty,i} \tag{17}$$

$$\hat{c}_{\infty,i} = \frac{q_0}{\Delta c_\infty} \exp\left(-\frac{\theta_s}{\theta}\right) \tag{18}$$

$$\hat{c}_i^* = \hat{c}_{\infty,i} \exp\left(\frac{\alpha_\theta}{\lambda\theta}\right) \tag{19}$$

Additionally, we obtain the rescaled initial conditions as follows:

$$\hat{\phi}_{3,0}^L = \frac{\phi_{3,0}^L}{\phi_r} = 1 \tag{20}$$

$$\hat{\phi}_{3,0}^D = \frac{\phi_{3,0}^D}{\phi_r} = \frac{1 + ee_0}{1 - ee_0} \tag{21}$$

$$S_{\infty,0} = 1 \tag{22}$$

It is worth noting that such formulation of the model equations highlights that the process depends, on one hand, on the operating conditions through the dissolution factor, which is determined by three parameters (linked to one another), that is, Δc_∞, ρ_0, and ee_0, with ee_0 also defining the initial conditions, and, on the other hand, by the system characteristics indicated by the four dimensionless parameters: θ_g, θ_r, θ_s, and α_θ. The first two are the rescaled activation energies of growth, $\theta_g = E_g/(RT_r)$, and racemization, $\theta_r = E_r/(RT_r)$, which account for the temperature dependency of their kinetics. The other two are related to the nominal solubility and to the capillary length, respectively, and are defined as $\theta_s = q_1/T_r$ and $\alpha_\theta = \alpha_0/(L_r T_r)$. On this basis, we will show in the following that the dissolution factor, δ_0, plays a primary role in determining the performance of the deracemization process, while the other parameters play only a secondary role.

The definition of the dissolution factor as a function of the initial conditions in eq 14 provides a design parameter, which indicates the deracemization capacity of a single cycle at the initial conditions of the suspension. Note that eq 14 links four quantities, three of which can be chosen independently to design the process, both in simulations and in experiments. The same dissolution factor can be computed during the process by using the current state of the suspension, that is, the values of the instantaneous enantiomeric excess, ee, and suspension density, ρ, for instance at the end of each cycle n, that is, at $T = T_{min}$, together with the value of Δc_∞ corresponding to the next cycle, $n + 1$. This quantity, indicated as δ_n, and its evolution inform us on how the cycle capacity

https://doi.org/10.1021/acs.oprd.1c00310
Org. Process Res. Dev. 2021, 25, 2551−2565

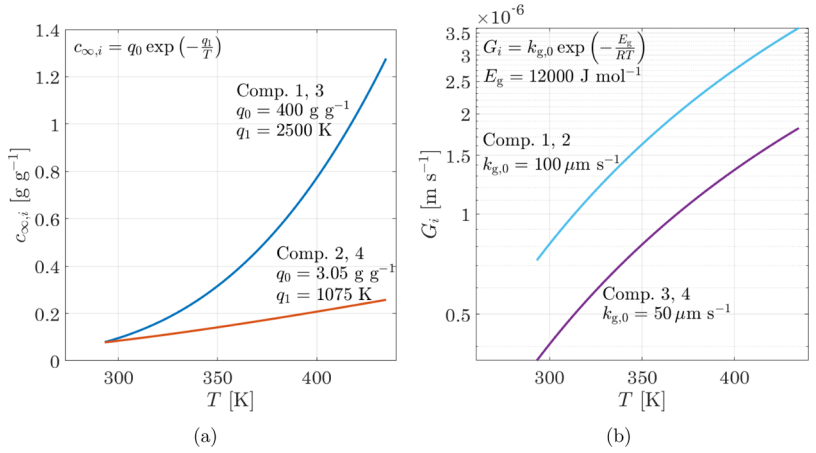

Figure 1. Properties of the compounds simulated as a function of temperature: (a) solubility curve (eq 3) and (b) growth rate (eq 5).

evolves during the process, thus enabling a better conceptualization of the process behavior. Moreover, it can be exploited to design deracemization processes with non-periodic cycles (Section 5), where the amount dissolved, Δc_∞, varies, in fact decreases, as the enantiomeric excess increases.

In any case, the dissolution ratio is defined based on thermodynamic solubility. Therefore, when it is larger than 1, it means that the cycle amplitude is too small to completely dissolve the distomer crystals. When the dissolution factor is close or equal to 1, the distomer amount dissolving, and thus the cycle capacity, is the largest. While when it is smaller than 1, the cycle amplitude is such that not only the distomer but also the eutomer dissolves until solubility is reached. In principle, this is not desired because the goal is to collect the target enantiomer in the solid phase. However, in practice, the actual distomer amount that dissolves can be smaller than that determined by the nominal solubility due to kinetic limitations. By replacing the latter with the former in eq 14, we obtain the effective dissolution factor, that is, δ_0^{eff} (δ_n^{eff}), which is larger than the set value, δ_0 (δ_n). It follows that even when setting the dissolution factor to a value smaller than 1, it may happen that in practice, $\delta_0^{\text{eff}} \geq 1$ ($\delta_n^{\text{eff}} \geq 1$), which can be beneficial for the deracemization process (Sections 4.4, 4.5, 5, and 5.1).

It is worth noting the interesting limit case of $\delta_0 = 0$ that corresponds to when $ee_0 = 1$. In this case, only eutomer seeds are present at the beginning of the process and a simple cooling crystallization with the racemization reaction occurring in solution is carried out. This simple and promising process variant was already introduced in previous works by other research groups[26,27] and will be thoroughly investigated in a dedicated paper in preparation.[28]

2.2. Simulation Conditions. In this work, we use the process model presented in Section 2.1 to investigate the effect of the dissolution factor, δ_0, on the deracemization process when the system characteristics vary. To this aim, we simulate the deracemization of four different compounds under several operating conditions. The four compounds differ two by two in solubility and growth rate constant, one faster (comp. 1−2) and one slower (comp. 3−4), as indicated in Figure 1b and Table 2. The two solubility functions differ both in absolute values, lower and higher, and because of their temperature dependence, stronger (comp. 1−3) or weaker (comp. 2−4) (Figure 1a and Table 2).

In a first set of simulations, we focus on modifying δ_0 by varying the initial suspension density, ρ_0, and the amount dissolved, Δc_∞. Additionally, we analyze how the initial dissolution factor affects the process when the minimum temperature is varied for each compound (see Table 3 for the parameters kept constant in the study and Table 4 for those varied). To avoid crystal washout, the inequality $\rho_0 - 2\Delta c_\infty > 0$ must be fulfilled; thus, the minimum threshold for the

Table 2. Parameters in the Equations Giving Solubility (Equation 3) and Growth Rate (Equation 5)[a]

		Solubility			
		q_0 [g g^{-1}]	q_1 [K]	q_0 [g g^{-1}]	q_1 [K]
Growth rate	$k_{g,0}$ [μm s^{-1}]	400	2500	3.05	1075
	100	Compound 1		Compound 2	
	50	Compound 3		Compound 4	

[a]In all cases, the activation energy in the growth rate expression is E_g = 12,000 J/mol.

Table 3. Initial, Operating, Compound-Specific, and Scaling Parameters Kept Constant in All Simulations

parameter			value
mean length and standard deviation	$L_{i,0}$, $\sigma_{i,0}$	[μm]	50, 0.05
heating, cooling rate	R_h, R_c	[K s^{-1}]	0.017, 0.0053
isothermal time	t_1, t_3	[s]	600
activation energy of growth	E_g	[J mol^{-1}]	1.2×10^4
activation energy of dissolution	E_d	[J mol^{-1}]	1.2×10^4
activation energy of racemization	E_r	[J mol^{-1}]	7.5×10^4
pre-exponential factor of dissolution	$k_{d,0}$	[μm s^{-1}]	200
pre-exponential factor of racemization	$k_{r,0}$	[s^{-1}]	10^{11}
surface shape factor	k_s	[-]	π
volume shape factor	k_v	[-]	$\pi/6$
crystal density	ρ_c	[kg m^{-3}]	1300
capillary length constant	α_0	[K m]	9.2×10^{-7}
universal gas constant	R	[J mol^{-1} K^{-1}]	8.314
reference length	L_r	[μm]	$t_r k_{g,0}$
reference temperature	T_r	[K]	273
reference time	t_r	[s]	$k_{r,0}^{-1}$
reference third moment	ϕ_r	[m^3]	$\phi_{3,0}^L$
reference concentration	c_r	[g g^{-1}]	$\Delta c_\infty = c_{\infty,i}(T_{max}) - c_{\infty,i}(T_{min})$

https://doi.org/10.1021/acs.oprd.1c00310
Org. Process Res. Dev. 2021, 25, 2551−2565

Table 4. Initial and Operating Conditions Varied in the Simulations[a]

parameter			value
dissolution factor	δ_0	[-]	0.8−3
initial suspension density	ρ_0	[g g^{-1}]	0.02−0.5
initial enantiomeric excess	ee_0	[-]	**0.4**, 0.2−0.8
amount dissolved	Δc_∞	[g g^{-1}]	0.02−0.16
minimum temperature	T_{min}	[K]	**293**, 298, 303
maximum temperature	T_{max}	[K]	$T_{max}(\Delta c_\infty, T_{min}) > T_{min} + 1$

[a]The values in bold are used as base cases.

suspension density at high temperature is set to 0.01 g g^{-1}. Moreover, a minimum cycle amplitude of 1 °C is selected, and each simulation is run until the ee reaches at least 0.95.

2.3. Non-periodic Temperature Cycles. As an alternative to the conventional periodic temperature profile, we performed temperature cycles with the same cooling rate but varying ΔT during the deracemization process. In such cycles, both the period and the amplitude of the cycle vary over time during the deracemization process; hence, they are referred to as "non-periodic cycles".

To simulate non-periodic temperature cycles, we have modified accordingly the code used to solve the mathematical model described in Section 2.1. The criterion on how to select the non-periodic cycles is that of modifying the temperature cycle amplitude during deracemization in order to keep the value of δ_n close to a chosen set point during the course of the deracemization process. The current value of δ_n is computed in each cycle from the distomer third moment and Δc_∞ currently set. If the difference between the set value and the current value of δ_n is larger than the given tolerance, the Δc_∞ is varied until the current δ_n is close enough to that set value. Larger and smaller deviations from the chosen value are allowed by, respectively, increasing and decreasing the tolerance value. Compound 1 is chosen to carry out this study; all the constraints defined for the periodic cycles are applied also in this case.

2.4. Performance Assessment. To evaluate the performance of the process investigated in this work, we refer to two different indicators. First, we examine the fundamental effects of the operating and system parameters by looking at the total number of cycles required to reach a minimum ee value of

Table 5. List of Experimental Conditions and Results

exp. [#]	δ_0 [-]	T_{min} [°C]	ΔT [°C]	Δc_∞ [×10^{-3} g g^{-1}]	ρ_0 [g g^{-1}]	n_{95} [#]	$t_{process}$ [h]	P [g kg^{-1} h^{-1}]
				NMPA				
n1	1.5	30	6.5	2	0.010	5	1.67	1.79
n2[a]	2	30	6.5	2	0.013	11	3.66	1.15
n3	2	30	11.8	4	0.027	9	3.61	2.22
n4	2	30	16.3	6	0.040	8[b]		
n5	3.5	30	6.5	2	0.023	20	6.66	1.04
n6	5	30	6.5	2	0.033	53[b]		
n7[c,d]	1.4	30	16.3	6	0.040	2	2.97	2.78
n8[d]	1.4	30	21.0	8	0.056	4[b]		
n9[d]	1.4	30	16.3	6	0.040	4[b]		
n10	1.5	25	7.6	2	0.010	5	1.73	1.61
n11	2	25	7.6	2	0.013	11	3.82	0.98
n12	2	25	13.6	4	0.027	9	3.81	1.94
n13	3.5	25	7.6	2	0.023	25	8.67	0.75
				Non-periodic Temperature Profile				
n20	2	30	6.5, 5, 3	2, 1.5, 0.9	0.013	6	2.50	1.38
n21	2	30	6.5, 3.5	2, 1	0.013	10	4.00	0.89
n22	2	30	varies	$\delta_n \approx 1.5$	0.013	17	6.00	0.63
				CPG				
c1	1.5	30	5.7	2	0.010	16	5.17	0.57
c2	2	30	5.7	2	0.013	20	6.46	0.61
c3	2	30	10.2	4	0.027	10	3.80	2.13
c5	3.5	30	5.7	2	0.023	26	8.40	0.82
c14	3.5	30	10.2	4	0.047	18	6.84	2.00
c11	2	25	7.0	2	0.013	15	5.11	0.81
c13	3.5	25	7.0	2	0.023	24	8.17	0.85
				tLEU				
t1	1.5	36	1.6	2	0.010	5	1.84	1.51
t15	1.5	36	3.0	4	0.020	5	2.40	2.70
t2	2	36	1.6	2	0.013	9	3.31	1.17
t3	2	36	3.0	4	0.027	7	3.35	2.62
t16	1.5	28	4.1	4	0.020	7	3.93	1.54
t11	2	28	2.1	2	0.013	10	4.12	0.97
t12	2	28	4.1	4	0.027	12	6.73	1.31

[a]Exp. n2bis was repeated at the same conditions, but with a different batch of material, leading to $t_{process}$ = 2.50 h and P = 1.41 kg^{-1} h^{-1}. [b]n_{95} is obtained from data extrapolation using the functional form $ee = ee_0 \exp kn_c$.[16,37] The process time and productivity are not reported as the ee never reaches 0.95. [c]R_c = 0.22 °C/min. [d]ee_0 = 0.6.

https://doi.org/10.1021/acs.oprd.1c00310
Org. Process Res. Dev. 2021, 25, 2551−2565

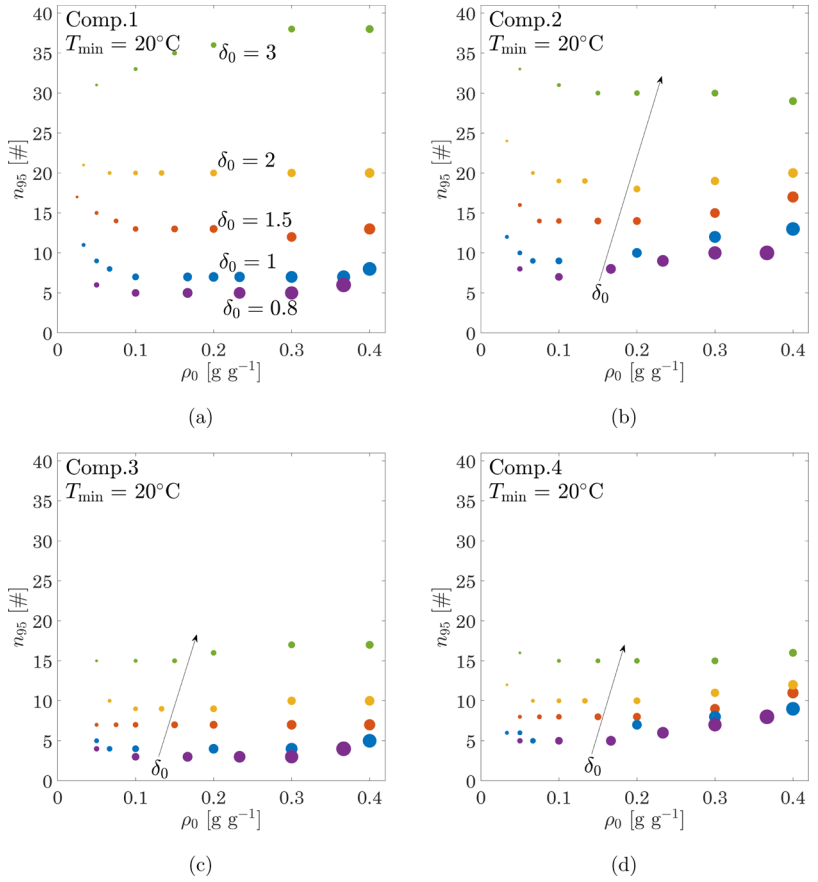

Figure 2. Effect of the initial suspension density, ρ_0, on the total number of cycles, n_{95}, at dissolution factor δ_0 = 0.8, 1, 1.5, 2, and 3 in purple, blue, red, yellow, and green, respectively, for the four compounds simulated [compounds 1−4, from (a−d)], with ee_0 = 0.4: top vs bottom row for faster vs slower growth and left vs right column for higher vs lower solubility. The marker size is proportional to Δc_∞.

0.95; we call this quantity n_{95}. Then, we assess how they affect the process performance by defining the productivity as follows (see eq 13 in an earlier paper[25]):

$$P = \frac{k_v \rho_c}{t_{process}}[(\phi^D_{3,final} - \phi^L_{3,final}) - (\phi^D_{3,0} - \phi^L_{3,0})] \left(3600 \times 1000\right)\left[\frac{g}{kgh}\right] \quad (23)$$

where $t_{process}$ is the total process time calculated as the sum of the cycle times of the n_{95} cycles, ϕ^D_3 is the third moment of the PSD, proportional to the crystal mass, of the desired enantiomer, and ϕ^L_3 is that of the undesired one at the beginning and the end of the process with subscripts "0" and "final", respectively.

3. EXPERIMENTAL SECTION

3.1. Material. The experiments presented in this work were performed with three different chemical systems already used in previous works investigating solid-state deracemization: *N*-(2-methylbenzylidene)-phenylglycine amide (NMPA),[12,29] 2-(benzylideneamino)-2-(2-chlorophenyl)acetamide (CPG),[30−32] and 3,3-dimethyl-2-((naphthalen-2-ylmethylene)amino) butanenitrile (tLEU).[13,33] These imine derivatives racemize in solution in the presence of the base 1,8-diazabicyclo-[5.4.0]undec-7-ene (DBU) as the racemizing agent. For NMPA and CPG, a 95 wt % mixture of 2-propanol (IPA) in acetonitrile (ACN) was used as a solvent, while for tLEU, pure methanol was selected. The compounds were synthesized according to the procedures reported in the literature;[31,34,35] the racemizing agent and the solvents were purchased from Sigma-Aldrich.

3.2. Experimental Protocol. Deracemization via temperature cycle experiments with periodic and non-periodic temperature profiles were performed at a small scale (1.8 mL) in a customized version of Crystal16 (Technobis).[36] The experimental and analytical protocols followed were those described in our previous works with NMPA,[12] CPG, and tLEU.[13]

In all cases, the temperature profile consists of four steps: one heating ramp, one cooling ramp, and two isothermal steps in between at the maximum temperature (T_{max}) and the minimum temperature (T_{min}). To shorten the process time, the duration of the isothermal step at high temperature was modified from 10 min (previous works) to 5 min (here) after verifying that this has a minor effect on the process outcome. At the beginning of the process, we suspended an enriched mixture of the two enantiomers in the crystalline form, previously prepared at the desired ee_0, in a saturated racemic solution, and the deracemization was run until an ee of 0.95 was reached; some experiments were terminated earlier than that for practical reasons (Section 3.3).

In deracemization via *periodic* temperature cycles, the amplitude of the temperature profile, ΔT, was kept constant and the experiments were performed as described in our previous works.[12,13,24] On the contrary, when *non-periodic*

https://doi.org/10.1021/acs.oprd.1c00310
Org. Process Res. Dev. 2021, 25, 2551−2565

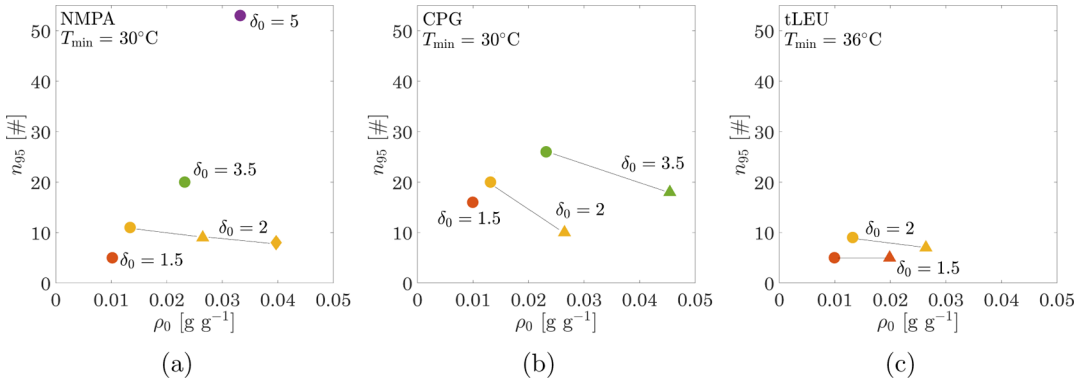

Figure 3. Effect of the initial suspension density, ρ_0, on the total number of cycles, n_{95}, for dissolution factor δ_0 = 1.5, 2, 3.5, and 5 in red, yellow, green, and purple, respectively, for experiments carried out with (a) NMPA, (b) CPG, and (c) tLEU. The value of Δc_∞ is indicated by the choice of symbol, namely, circles, triangles, and diamonds, for Δc_∞ = 0.002, 0.004, and 0.006 g g^{-1}, respectively. For the experiments performed with NMPA at δ_0 = 2 and ρ_0 = 0.04, and δ_0 = 5, the n_{95} is obtained from data extrapolation using the functional form $ee = ee_0 \exp(kn_c)$.[16,37]

temperature cycles were performed, the cycle amplitude (ΔT) was gradually reduced during the process. To do this, two alternative approaches were implemented: (i) the profile was set a priori; (ii) the temperature amplitude was modified according to the latest value of ee obtained by HPLC analysis: the ee was used to compute the Δc_∞, that is, the value of ΔT, so as $\delta_n = \rho(1 - ee)/(2\Delta c_\infty)$, corresponded to a set value. We assumed that the suspension density at the minimum temperature was constant during the process, that is, $\rho = \rho_0$, while the ee corresponds to the measured value at the end of the cycle.

3.3. Experimental Conditions. Table 5 reports the conditions of the experimental runs, together with the observed total number of cycles, n_{95}, and the calculated process productivity. The two performance indicators are given as the mean value of the results of three experiments (only two in exp. n7 and n8) repeated at the same conditions to verify reproducibility, which is indicated by the overlapping of the ee data of the repetitions illustrated in Figures 9, 10, and 13a. It is worth noting that in some experiments with NMPA, the ee did not reach 0.95 because of a very long process time (exp. n6) or because the ee plateaus to a lower value without evolving any further (exps. n4, n8, and n9; for a discussion thereof, see Section 4.5). If not explicitly stated, the ee_0 is set to 0.4 and the heating/cooling rate to 1.3 °C/min, except for the case of tLEU, where the reference cooling rate is 0.22 °C/min. The parameters varied are the dissolution factor (δ_0), the amount dissolved (Δc_∞), the initial suspension density (ρ_0), and the minimum temperature of the cycle (T_{min}), while the DBU concentration is kept constant (6 μL g^{-1}). The design of the experimental campaign is based on the same criteria and constraints described in Section 2.2 for the simulations.

4. RESULTS ON PERIODIC TEMPERATURE CYCLES

In this section, we present the results obtained in the case of the deracemization via periodic temperature cycles of different (real and virtual) compounds with a particular focus on the role of the initial dissolution factor. To elucidate this, we compare qualitatively the experimental measurements and the simulated results. We exploit the mathematical model to isolate the effects of different system properties, thus gaining insights on the system behavior and enabling the rationalization of the experimental trends. It is worth noting that the simulations in this work do not account for nucleation, breakage, and agglomeration. While these phenomena may obviously occur in the experiments, we have selected operating conditions that should minimize their occurrence.

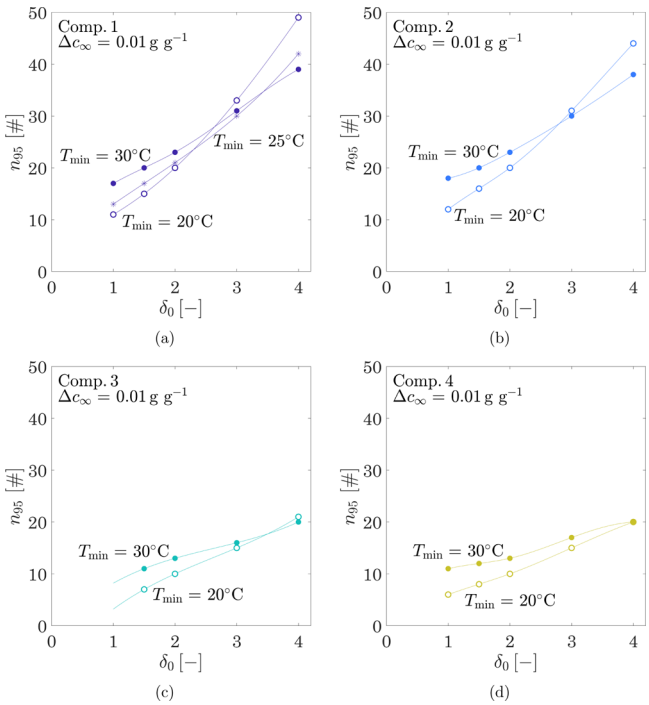

Figure 4. Effect of temperature, T_{min}, on the total number of cycles, n_{95}, as a function of the dissolution factor, δ_0, for the four simulated compounds [compounds 1−4, from (a−d)]. The lines are guides to the eye.

In the following, we, first, present the simulation results to clarify the effect of δ_0 on the process by varying its value as well as by keeping it constant when Δc_∞ and ρ_0 change accordingly. Second, we demonstrate that similar trends are obtained in the experiments (listed in Table 5). Third, we analyze the effect of the system kinetics by varying the temperature range. Then, we evaluate the process productivity as a function of the initial conditions, namely, the δ_0, the ee_0, and the ρ_0. Finally, with the aid of the process model, we discuss some selected experimental results that appear to deviate from the expected behavior.

https://doi.org/10.1021/acs.oprd.1c00310
Org. Process Res. Dev. 2021, 25, 2551−2565

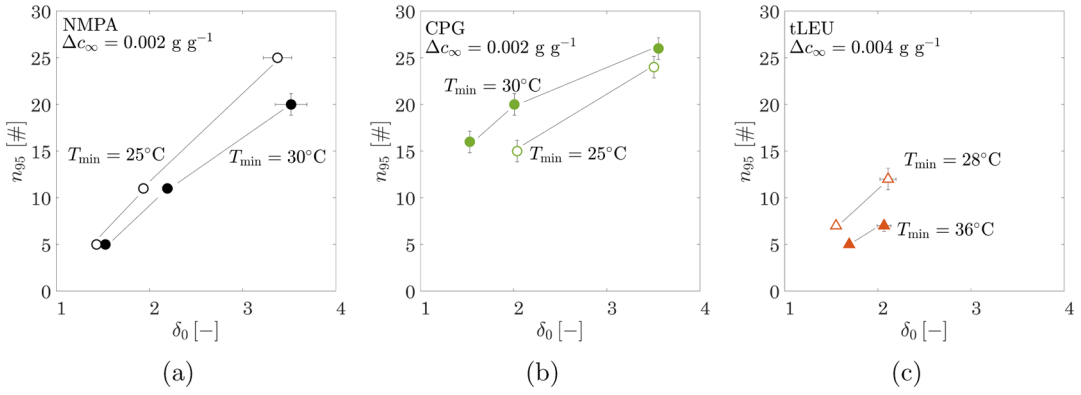

Figure 5. Effect of temperature as a function of the dissolution factor, δ_0, on the total number of cycles, n_{95}, for the deracemization of the three experimental systems: NMPA, CPG, and tLEU, (a), (b), and (c), respectively, at different minimum temperatures, T_{min}. The error bars correspond to the standard deviation of the n_{95} (vertical) and that of the dissolution factor (horizontal) obtained from three repetitions of the same experiment. The lines are guides to the eye.

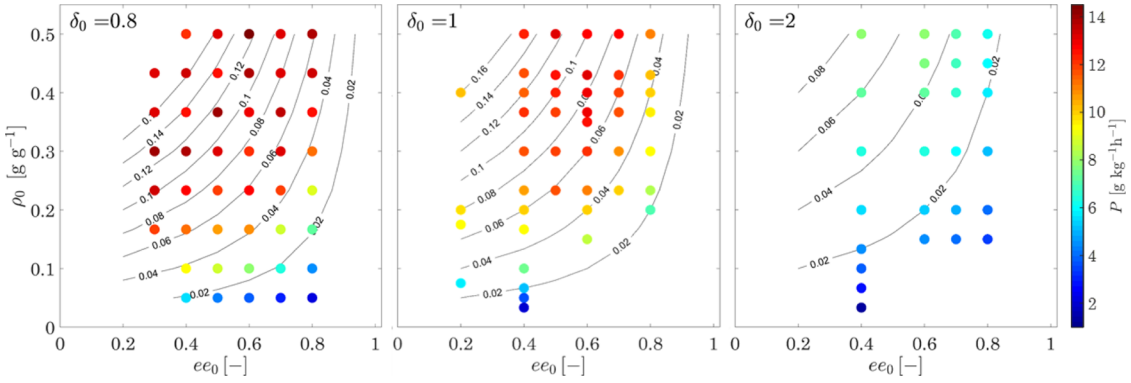

Figure 6. Productivity (color code) of the deracemization process of compound 1 at T_{min} = 20 °C as a function of ee_0 and ρ_0 for δ_0 = 0.8, 1, 2, from left to right. The contour lines indicate how the Δc_∞ ([g g^{-1}]) varies in the $ee_0 - \rho_0$ plane so as to keep constant the chosen value of δ_0.

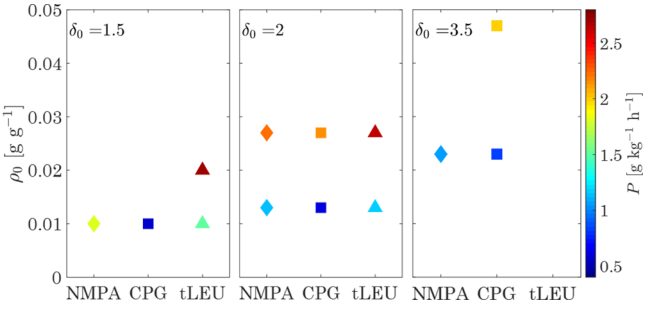

Figure 7. Productivity (color code) as a function of ρ_0 for δ_0 increasing from left to right of the experiments with NMPA (diamonds), CPG (squares), and tLEU (triangles), performed at the high temperature level, T_{min}, with ee_0 = 0.4.

4.1. Simulation Results. The results of the simulation study carried out with the four compounds introduced in Section 2.2 allow to define a conceptual framework for the understanding and design of deracemization processes based on temperature cycles. In Figure 2, we show the total number of cycles, n_{95}, as a function of the initial suspension density for different values of dissolution factor, namely, 0.8, 1, 1.5, 2, and 3 (using purple, blue, red, yellow, and green markers, respectively). The size of the markers is proportional to the amount dissolved, Δc_∞, to underline how this quantity is related to ρ_0 at constant values of δ_0. The latter is varied up to 0.4 g g^{-1} to include the consideration of highly concentrated slurries, typical of some industrial applications.

The simulation results demonstrate two main effects of the initial value of the dissolution factor: (i) for a given value of δ_0, the number of cycles remains rather constant when ρ_0 and Δc_∞ vary accordingly; (ii) the total number of cycles decreases with decreasing δ_0, thus showing that the limit case whereby $\delta_0 = 0$ may have potential.[28]

By simulating the four different compounds presented in Section 2.2, we observe that the dissolution factor affects their deracemization similarly. Particularly, we exploit the process model to examine effects that cannot be easily decoupled experimentally, such as how either different growth rates or solubility curves selectively affect the deracemization. It can be readily observed that the effect of the growth rate (Figure 2, top—faster growth—vs bottom row—slower growth) is stronger than that of the solubility (Figure 2, left—higher solubility—vs right column—lower solubility). This suggests that the former plays a more important role than the latter, at least when racemization is not the limiting phenomenon. With a lower growth rate, the target enantiomer grows preferentially because its total surface area is larger than that of the distomer, whose supersaturation is consumed more by the racemization reaction rather than by crystal growth. On the contrary, when the growth rate is higher, the competition between the two phenomena favors not only the distomer racemization but also its growth, thus slowing down the deracemization process. When the solubility has a weaker temperature dependence, for

https://doi.org/10.1021/acs.oprd.1c00310
Org. Process Res. Dev. 2021, 25, 2551−2565

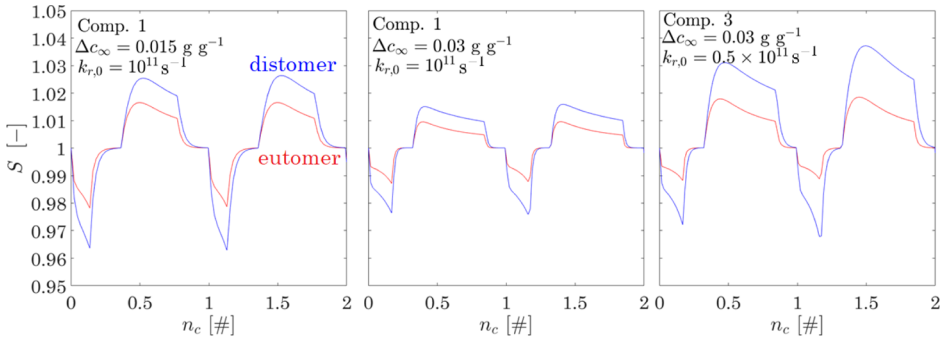

Figure 8. Simulated supersaturation profiles of the distomer (blue) and eutomer (red) in the first two deracemization cycles, n_c, at T_{min} = 20 °C, ee_0 = 0.4, and δ_0 = 1, for compound 1 (lhs, middle) and compound 3 with slow racemization kinetics (rhs).

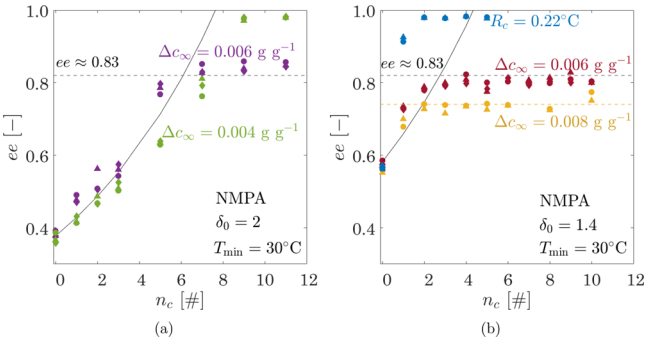

Figure 9. Effect of the amount dissolved, Δc_∞, for NMPA in (a) exps. n3, at Δc_∞ = 0.004 g g^{-1}, and n4, Δc_∞ = 0.006 g g^{-1}, in green and purple symbols, respectively; (b) exps. n7 and n9, with Δc_∞ = 0.006 g g^{-1}, in blue and red, respectively, and exp. n7 at Δc_∞ = 0.008 g g^{-1} in yellow. The full lines show the data fit with the equation $ee = ee_0 \exp kn_c$,[16,37] and the dashed lines underline the value of the ee at the plateau. The y-axis was adapted for clarity.

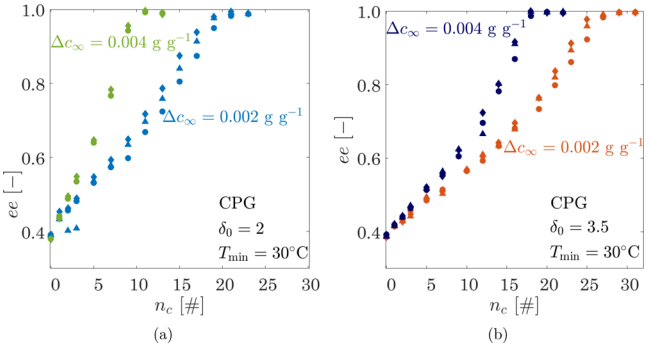

Figure 10. Effect of the amount dissolved, Δc_∞, for CPG at (a) δ_0 = 2, exps. c2, c3 in blue and green, respectively, and (b) δ_0 = 3.5, CPG exp. c5 and c14 in orange and blue, respectively. The y-axis was adapted for clarity.

a given T_{min}, a larger value of ΔT and hence a higher T_{max} are needed to attain a specific value of Δc_∞. Nevertheless, we observed that such a high temperature level has a minor effect on the process as compounds with different temperature dependences of solubility deracemize in a similar number of cycles (Figure 2, left vs right column). Note however that in this case, the cycle time and the corresponding total process time are longer with larger ΔT.

4.2. Experimental Runs. The experimental results obtained with NMPA, CPG, and tLEU are illustrated in Figure 3a, b, and c, respectively. The total number of cycles,

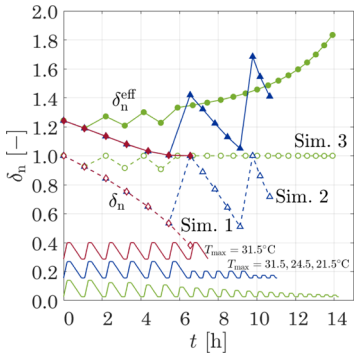

Figure 11. Dissolution factor computed from the nominal, δ_n (open symbols), and the effective, δ_n^{eff} (open symbols), amount dissolved as a function of time for periodic (sim. 1, red) and non-periodic cycles (sim. 2 and 3, blue and green, respectively). A scaled version of the corresponding temperature profile is reported at the bottom.

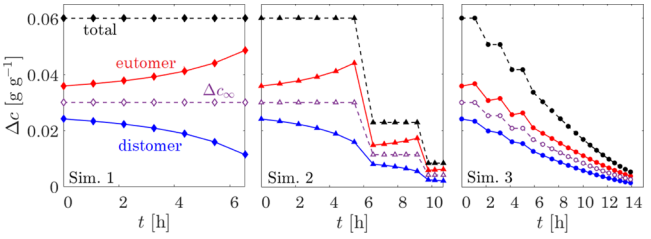

Figure 12. Amounts dissolved in sim. 1, 2, and 3 from left to right: total (black symbols), eutomer (red, solid line), and distomer (blue, solid line); total set value (dashed black line) and single enantiomer nominal value, Δc_∞ (purple, dashed line).

n_{95}, is plotted as a function of the initial suspension density, ρ_0, for different values of the dissolution factor, which correspond to different values of Δc_∞ as indicated by the different colors and symbols used for the markers in Figure 3 (see the explanation in the corresponding caption).

These experimental results generally agree with the simulation trends described above. First, rather similar n_{95} values are obtained in experiments where the initial dissolution factor is kept constant, while the initial suspension density and the amount dissolved vary accordingly. This effect is clearly observed with NMPA at δ_0 = 2, yellow symbols in Figure 3a (exp. n2, n3, and n4), and with tLEU in Figure 3c both at δ_0 = 1.5 (exp. t1 and t15) and at δ_0 = 2 (exp. t2 and t3). In the case of CPG, for δ_0 = 2 and 3.5, there is a major difference in the n_{95} values at different initial suspension densities; this anomalous behavior is discussed in depth and rationalized in Section 4.5.

https://doi.org/10.1021/acs.oprd.1c00310
Org. Process Res. Dev. 2021, 25, 2551−2565

In the same section, also, the peculiar pattern that characterizes exp. n4 is examined.

Second, when δ_0 increases, the number of cycles, n_{95}, increases as well, as clearly observed in the case of NMPA, when δ_0 varies from 1.5 to 2, to 3.5, and to 5, in exps. n1, n2, n5, and n6, respectively (Δc_∞ = 0.002 g g^{-1}, circles). This effect is general and can also be observed in the case of CPG and tLEU.

4.3. Effect of Temperature Levels. The objective of this section is to study the effect of changing those model parameters that can be varied while modifying neither δ_0, nor Δc_∞, nor ρ_0. After rescaling the model equations, besides δ_0, the only parameters left are those that characterize the temperature dependence of the rate constants of racemization and growth as well as of the pre-exponential term in the solubility relationship and of the capillary effect. Changing the operating temperature range at constant Δc_∞, that is, by changing T_{min} and adjusting T_{max} so as to keep the same value of Δc_∞, allows analyzing the combined effect of all these parameters at once. The simulations and the experimental results are illustrated in Figures 4 and 5, respectively, where for the four virtual compounds already considered above and for the three experimental compounds, we plot the total number of cycles, n_{95}, as a function of the dissolution factor for different levels of the minimum temperature (at the same value of Δc_∞ as indicated in each plot).

The results of simulations carried out at different values of T_{min} (Figure 4) confirm for all compounds that the number of cycles increases with increasing value of the dissolution factor; this is the primary effect already discussed in Sections 4.1 and 4.2. As a secondary effect, we observe that at low δ_0 values, the deracemization is faster when the minimum temperature is lower, T_{min} = 20 °C, whereas the opposite occurs beyond a compound-specific δ_0 threshold. Thus summarizing, low δ_0 values and low temperature levels yield the smallest number of temperature cycles for complete deracemization.

These trends are also confirmed in experiments, although experimental runs exhibit compound-specific effects. With NMPA (Figure 5a), the number of cycles of experiments performed at different T_{min} is the same when δ_0 has a low value (δ_0 = 1.5 in exps. n1 and n10, and δ_0 = 2 in exps. n1 and n11), but when it increases (δ_0 = 3.5 in exps. n5 and n13), the process needs fewer cycles at a high temperature level, as indicated by the simulations with compounds 1 and 2 (Figure 4a,b). For tLEU, the deracemization is promoted by high temperature already when δ_0 = 1.5 (exps. t15 and t16 in Figure 5c), while with CPG, a low temperature range is beneficial in all experiments (Figure 5b). However, one notices that the difference between the n_{95} values at low and high T_{min} becomes smaller as δ_0 increases, resembling the trend exhibited by the simulations with compounds 3 and 4 (Figure 4c,d).

The trends shown in the figures above can be rationalized by keeping in mind that the dissolution factor is by definition a measure of the theoretical efficiency of the cycle, which is higher for low values of δ_0. It is worth noting that the amount of the distomer dissolved was kept constant in the cases compared; thus, low and high values of δ_0 correspond, respectively, to small and large amounts of the distomer to deracemize. The different distomer amount present combined with higher and lower cycle efficiencies given by the value of δ_0 is responsible for the observed trends. Let us consider the case when the minimum temperature is low and hence, the kinetics are slow. Under such conditions, at low values of the dissolution factor, a large fraction of the counter enantiomer dissolves and racemizes upon heating. Therefore, the larger amount of eutomer crystals at T_{max} can grow slowly but preferentially, thus leading to fast deracemization. When the δ_0 increases, the decrease of the temperature cycle efficiency combined with the slow kinetics is responsible for a long process. On the contrary, when operating in a high-temperature range, the fast kinetics promotes competition of racemization and growth between the two enantiomers, thus delaying the process at low values of the dissolution factor. However, at higher values of δ_0, fast kinetics compensates for the low cycle efficiency, thus promoting a faster process.

All experimental data presented here are novel and have been obtained specifically for this work. In our earlier work on the effect of temperature range and system kinetics, we showed that the process is fostered at a high-temperature range for NMPA and tLEU. The behavior of CPG, however, showed a weak temperature dependence (the number of cycles to deracemize first slightly increased and then slightly decreased with increasing minimum temperature as shown in Figure 8[13]). By analyzing these results with the help of the parameter δ_0 introduced in this work, we can conclude that the runs with NMPA and tLEU were carried out at a value of δ_0 for which a high-temperature range promotes faster deracemization, while for CPG, the value of the dissolution factor was close to that leading to a similar number of cycles for different temperature levels. In conclusion, the trends reported in earlier papers[12,13] are fully consistent with the analysis presented here and could in principle be reported on the same diagrams of Figures 3 and 5. However, in practice, they have been obtained under slightly different conditions, such as different ee_0 and DBU concentrations, and with different batches of the material; hence, they are not exactly comparable and are not reported for simplicity.

4.4. Productivity Assessment. In this section, we look at the process productivity defined by eq 23 as a function of the dissolution factor as well as of the initial suspension density, ρ_0, and of the initial enantiomeric excess, ee_0, similar to previous works.[12,16,25] We select three values of δ_0 (0.8, 1, 2) and simulate the deracemization of compound 1 for different combinations of ee_0 and ρ_0 that fulfill the design constraints described in Section 2.2. Note that based on such constraints, the area of the ee_0−ρ_0 plane that is feasible becomes smaller when δ_0 decreases.

Considering the color code used in Figure 6, one can readily observe that the largest productivity is attained when the dissolution factor equals 0.8 [Figure 6, left-hand side (lhs)]. Moreover, at low values of δ_0, there are more combinations of values of ee_0 and ρ_0 resulting in high productivity, for example, larger than 12 g kg^{-1} h^{-1}. As a consequence, more beneficial conditions for the process can be found at lower values of the dissolution factor than at higher ones. As already illustrated in Figure 8 of a previous work,[25] the productivity does not increase monotonically with ee_0 and ρ_0, but a maximum value can be found. In our case, this corresponds to a productivity of 14.3 g kg^{-1} h^{-1}, when ee_0 = 0.6 and ρ_0= 0.5 g g^{-1}.

By examining the productivity of experiments carried out with ee_0 = 0.4, reported for the different compounds in Figure 7, we observe once again that the process performance is favored at low values of initial dissolution factor for a given suspension density. Additionally, high suspension densities lead to higher productivity values, thus indicating that we operate at ρ_0 levels below those attaining optimal productivity.

https://doi.org/10.1021/acs.oprd.1c00310
Org. Process Res. Dev. 2021, 25, 2551−2565

Therefore, when designing a new deracemization process, one should choose a low δ_0 value and perform a couple of screening experiments at different ee_0 and ρ_0 levels to identify how these operating parameters must be varied to achieve the most productive conditions.

From the analysis of the effect of the dissolution factor on the productivity, we conclude that the process performance can be improved by either operating at the lowest possible value of the dissolution factor, that is, $\delta_0 = 0$, when $ee_0 = 1$, as anticipated in Section 2.1 and thoroughly analyzed in its advantages and disadvantages in a dedicated work (in preparation),[28] or applying non-periodic cycles, where the amplitude of the temperature cycles, and thus the Δc_∞, is modified during the process, such that the dissolution factor is set for each cycle to a desired low value. The design and the potential benefits of this approach are discussed in Section 5.

4.5. Special Cases: Effect of Supersaturation. In this section, we analyze a few experimental runs that deviate from the trends presented above due to compound-specific thermodynamic and kinetic features. Specifically, we refer to (i) the experiments carried out with NMPA, where the deracemization stops at a certain value of ee without reaching complete deracemization, that is, where ee = 1, regardless of the value of initial enantiomeric excess used (exp. n4 in Figure 9a and exp. n8 and n9 in Figure 9b), and (ii) two pairs of experiments with CPG, that is, at $\delta_0 = 2$ (exps. c2 and c3, in Figure 10a) and $\delta_0 = 3.5$ (exp. c5 and c14, in Figure 10b), already presented in Figure 3b with yellow and green symbols, respectively. Although in these runs the number of cycles is expected to be constant for each value of δ_0, the deracemization is faster when the amount dissolved, and thus ρ_0, is larger.

We rationalize these observations by considering the maximum enantiomer amount that can be dissolved in each cycle, that is, Δc_∞. Depending on the system kinetics, a large value of Δc_∞, and hence of ρ_0 at constant δ_0, can enhance the preferential growth of the desired enantiomer and the fast racemization of the undesired one, thus promoting the consumption of the supersaturation for both enantiomers, which is kept at low levels. On the other hand, if the growth and racemization kinetics are not fast enough, the supersaturation increases to a range that can potentially lead to nucleation and growth of the undesired enantiomer, thus hindering deracemization and making the completion of the process impossible.

To verify this theory, we analyze the simulated supersaturation profiles of each enantiomer in the first couple of cycles under selected deracemization conditions, bearing in mind that the process model does not account for nucleation. When Δc_∞ increases at given δ_0, the supersaturation of both enantiomers becomes lower (Figure 8, left panel vs middle panel), thus suggesting that racemization and growth are more effective in maintaining low supersaturation values under these conditions. However, by simulating the deracemization of a slow growing system (compound 3) with slow racemization kinetics, that is, $k_{r,0} = 0.5 \times 10^{11}$ s^{-1}, under the same operating conditions, one notices that the supersaturation reaches higher levels, which can potentially promote nucleation and growth of the distomer (Figure 8, right panel).

This effect is observed when the value of Δc_∞ is increased from 0.004 g g^{-1} in experiment n3 to 0.006 g g^{-1} in experiment n4 (green and purple symbols, respectively, in Figure 9a). In the latter experiment, the enantiomeric excess increases until reaching a plateau at about 0.83. The same happens when the same Δc_∞ is applied to a suspension with $ee_0 = 0.6$ in experiment n9 (Figure 9b, red symbols), and the nucleation effect is enhanced by further increasing Δc_∞ in experiment n8 (Figure 9b, yellow symbols). By reducing the cooling rate, and hence the supersaturation, from 1.30 to 0.22 °C/min (exp. n7, blue symbols), enantiopurity is achieved quite rapidly, thus suggesting that the supersaturation level has a primary effect and promotes nucleation of the distomer. On the contrary, in the case of CPG, the faster deracemization attained upon the increase of the amount dissolved indicates that growth plays a major role at both δ_0 values evaluated (Figure 10).

5. RESULTS ON NON-PERIODIC TEMPERATURE CYCLES

To verify if the performance of the deracemization process improves when a non-periodic temperature profile is implemented, we examine simulations and experiments carried out by varying the amplitude of the cycle during the process.

5.1. Simulation Results. First, we exploit the process model to simulate the deracemization process with three types of temperature profiles (Table 6): (i) a standard periodic profile used as a reference case in sim. 1 (plotted in the lower part of Figure 11, in red); (ii) a non-periodic profile with T_{max} varying from 31.5 to 24.5 to 21.5 °C in a predetermined manner, in sim. 2 (blue profile); and (iii) a non-periodic profile where the constraint that $\delta_n = 1$ at every cycle allows calculating the maximum temperature of the next cycle by computing the desired Δc_∞ during the process from the ee and the suspension density measured at the end of the previous cycle (see sim. 3, i.e., the green profile in the figure).

Table 6. Simulation Conditions and Results of the Deracemization of Compound 1[a]

sim.	δ_0 [-]	ΔT [°C]	ee_0 [-]	$t_{process}$ [h]
1	1	11.5	0.4	7
2	1	11.5 (6), 4.5 (5), 1.5 (3)	0.4	11
3	1	varying such that $\delta_n \approx 1$	0.4	14
4	1.5	varying from 13 to 2	0.001	>78 (>270)
5	1.5	13	0.001	76 (267)
6	1.1	17	0.001	50 (178)
7	1.2	15	0.001	60 (206)
8	1.9	11	0.001	89 (326)
9	2.2	9	0.001	112 (362)

[a]In all cases, T_{min} = 20 °C, ρ_0 = 0.1 g g^{-1}, and R_c = 0.32 °C/min. Simulations from 4 to 9 are repeated with R_c = 0.05 °C/min, and the resulting process time is reported in brackets.

The simulation results are discussed by looking at the cycle dissolution factor, computed based on the solubility, that is, δ_n (open symbols with a dashed line), and on the actual amount of distomer dissolved in each cycle obtained from the simulation data, that is, δ_n^{eff} (full symbols, solid line). They are reported as a function of process time with the corresponding colors and symbols in Figure 11.

We observe that the process takes the shortest time in sim. 1, when δ_n monotonically decreases (7 h, red), while the delay observed in sim. 2 is a consequence of the increase of this parameter when the maximum temperature decreases (11 h, blue). In sim. 3, δ_n is kept constant on purpose, thus leading to the longest process time (14 h, green). When analyzing the value of δ_n^{eff}, one observes that it is always larger than the set

https://doi.org/10.1021/acs.oprd.1c00310
Org. Process Res. Dev. 2021, 25, 2551−2565

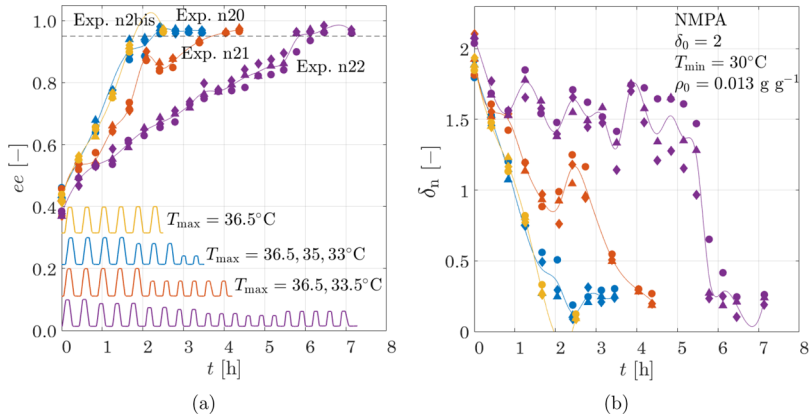

Figure 13. Experimental results of non-periodic cycles deracemization in yellow, blue, red, and purple for experiments n2bis (periodic), n20, n21, and n22, respectively: (a) evolution of the enantiomeric excess and the corresponding scaled temperature profile; (b) value of the dissolution factor over time. The lines are a guide to the eye.

value, δ_n, because the system kinetics play a role in determining how much of each enantiomer dissolves, and this deviates from the expected behavior. It is worth noting that this trend indicates that the amount of undesired enantiomer dissolved is lower than what was expected while designing the process. This kinetic effect is negligible in sim. 1 because the trends are the same for the δ_n and δ_n^{eff} values because of the periodic temperature cycles implemented in this case. However, it becomes relevant in sim. 2 and, particularly, in sim 3 because the δ_n^{eff} values increase more than expected when the cycle amplitude is modified, thus slowing the process down.

As mentioned above, the rationale behind this effect is the actual amount of each enantiomer dissolved, which is shown as a function of time with respect to the set Δc_∞ value (purple open symbols) in Figure 12 for sim. 1, 2, and 3 from left to right. It is evident that the kinetics and the size-dependent solubility foster the dissolution of the eutomer (full red symbols) at the expenses of that of the distomer (full blue symbols), which is lower than expected, thus leading to a value of the δ_n^{eff} larger than the set value, δ_n. Note that the total amount that should dissolve based on solubility (black dashed line) and that obtained from the simulation results (black full symbols) match. When a periodic profile is performed, the amount of eutomer (distomer) dissolved in the cycle increases (decreases) during the process because its amount and surface increase (decrease), while the enantiomeric excess evolves toward 1, thus promoting (hindering) its dissolution (Figure 12 left). On the contrary, when the cycle amplitude is reduced over the process, the driving force for dissolution decreases, thus resulting in a smaller amount of both species dissolved (Figure 12, middle and right).

5.2. Experimental Results. The evolution of the enantiomeric excess of selected experiments and the corresponding scaled temperature profile are reported with the corresponding color in Figure 13a (Table 5). Similarly, the values of the dissolution factor during the process, δ_n, are plotted in Figure 13b. For comparison with the non-periodic temperature profiles, experiment n2bis (yellow symbols) is run in parallel with a periodic temperature cycle. Although the operating conditions are those of exp. n2 (Table 5, Figures 3a and 5a), the deracemization time differs due to the different batch of solid and solvent mixtures employed. These materials are those used in the experiments where a non-periodic temperature profile is applied; thus, experiment n2bis is selected for a more reliable comparative analysis. In experiment n20 (blue symbols), the temperature profile is set a priori such that the maximum temperature varies from 36.5 to 35 and to 33 °C to reduce the cycle time. In spite of this, the same total deracemization time is observed in experiments n2bis and n20. This result is rationalized by looking at the value of the dissolution factor during the process: it decreases similarly for both experiments, suggesting that the deracemization proceeds at a very similar rate. On the contrary, in experiment n21 (red) the deracemization takes longer because the δ_n value first decreases and then increases; thus, the ee drops, when the amplitude of the cycle is reduced (T_{max} from 36.5 to 33.5 °C). The longest process time corresponds to exp. n22 (purple), where the temperature profile is modified cycle-by-cycle to keep the δ_n value around 1.5, based on the previous value of ee measured by HPLC analysis. In this case, deracemization is achieved only after increasing T_{max}, thus leading to the decrease of δ_n.

5.3. Previous Results in the Literature. From the experimental data and the simulation results, we conclude that carrying out non-periodic cycles does not particularly improve the performance of the deracemization via the temperature cycle process. This finding appears to be in contradiction with a previous contribution by Coquerel and co-workers,[21] where the authors suggested that by damping the temperature profile, that is, by reducing the cycle amplitude (they refer to their exps. III and V), deracemization is attained in a shorter time than when a periodic profile is applied (this occurs in their exps. IV and VI). We discuss this discrepancy in the following, where we refer to these experiments with the same roman numbers used in the original work that distinguish them from those presented here.

The first important consideration is that Suwannasang et al. started their experiments with a racemic solid, that is, $ee_0 = 0$. It is known that such a condition not only promotes a long deracemization process but also increases the variability of the total process time, which is instead reduced by introducing an initial bias asymmetry through a value of ee_0 larger than 0.[25,38] As a consequence, it can hardly be established if the different process time is due to this effect or to the type of temperature profile applied. Particularly questionable cases are those where the difference in process duration is not large, such as in exp. III, which takes only about 25% more time than exp. IV (31 and 24 h, respectively).

https://doi.org/10.1021/acs.oprd.1c00310
Org. Process Res. Dev. 2021, 25, 2551−2565

For the second set of experiments, damping the cycles in exp. VI (30 h) results in half the process time of exp. V, where the profile is periodic (60 h). However, in this case, the amplitude of the non-periodic cycles was initially twice as large as that of the periodic ones, that is, 10 °C instead of 5 °C. The authors suggested that the different ΔT may exaggerate the benefit of the non-periodic cycle. Here, we rationalize this effect by using the prior data to compute the dissolution factor, which is plotted over time together with the corresponding ee in Figure 14. We found that because of the different ΔT value,

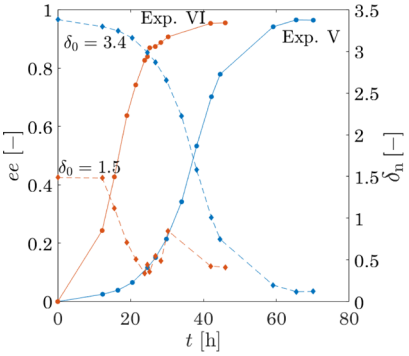

Figure 14. Enantiomeric excess (circle, full line) and dissolution factor (diamonds, dashed line) of the experiments by Suwannasang et al.[21] when periodic (blue, exp. V) and non-periodic cycles (red exp. VI) are performed. Note that the data from the previous publication are replotted here for the purpose of this work.

δ_0 is smaller in exp. VI, δ_0 = 1.5, than in exp. V, δ_0 = 3.4. According to the results presented in Sections 4.1 and 4.2, we must argue that this effect plays the key role in shortening the process time, thus masking the real effect of the non-periodic cycle profile (exp. VI).

To verify this conclusion, we run ad hoc simulations with $ee_0 \approx 0$ by setting ee_0 = 0.001, with different non-periodic temperature profile cycles (sim. 4, Figure 15 red symbols), and we compare the results with cases when periodic cycles with equal (sim. 5), larger (sim. 6 and 7), and smaller (sim. 8 and 9) cycle amplitudes are applied, that is, at equal, smaller, and larger δ_0 values, respectively. The simulation conditions and the corresponding results are summarized in Table 6 and illustrated in Figure 15; they confirm that the process takes the shortest time when the ΔT is the largest (sim. 6) and that for a given ΔT, the periodic cycles are more efficient (sim. 5) than the non-periodic ones (sim. 4). The latter is faster than sim. 8 and 9, where the cycle amplitude is smaller. This trend is a consequence of the value of δ_0, which is smaller when the ΔT is larger.

We repeated simulations 4–9 with cycles characterized by a slower cooling rate, that is, R_c = 0.05 °C/min, to investigate if the non-periodic temperature profile can become convenient in the case of processes with particularly long cycles. Figure 15b shows such a case when the cooling and heating ramps have a major weight in determining the cycle time; thus, the decrease of the ΔT is expected to be advantageous. Nonetheless, periodic temperature cycles perform better than non-periodic ones as long as the value of δ_0 is appropriately selected.

These results clearly show that a short deracemization time is achieved when operating at low values of the dissolution factor, which correspond to large values of the cycle amplitude, ΔT. At a given δ_0 level, the fastest process is attained when the cycles are periodic, that is, when the cycle amplitude is set to the maximum achievable value during the entire process. Therefore, reducing the ΔT to values smaller than that is sub-optimal, while applying periodic temperature cycles is indeed the most effective strategy. Moreover, a periodic temperature cycle process is simpler to design based on the information provided by the dissolution factor.

6. CONCLUDING REMARKS

The literature, including contributions from our group, has indicated that deracemization via temperature cycles has the potential to be the batch process for enantiomer purification exhibiting the simplest operation and the simplest reactor configuration. We have been able to show through experiments with a variety of compounds that it is a reproducible and robust process[12,13,24] and through simulations that operating conditions can be tuned rationally to improve process performance.[14,25] Nevertheless, it has also been apparent that deracemization via temperature cycles has very many degrees of freedom (in its periodic implementation; even more in the non-periodic implementation) that determine its performance, which is in turn dependent on many system parameters, of both a thermodynamic and kinetic nature. When facing the

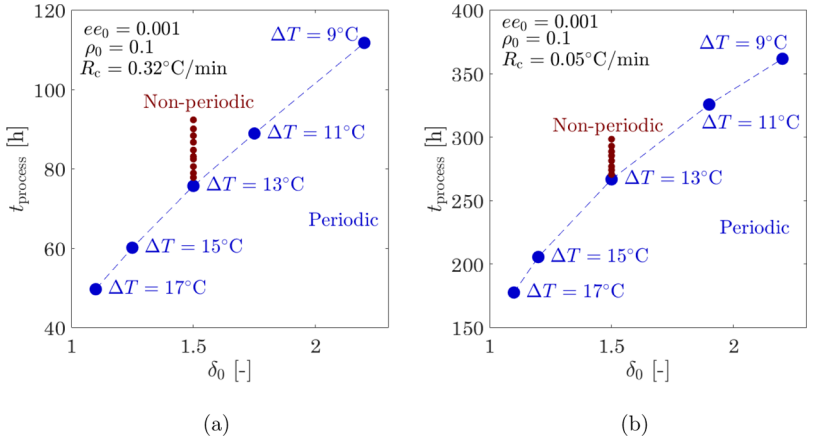

Figure 15. Comparison among deracemization via periodic (blue) and non-periodic (red) temperature cycles: simulated process time as a function of the dissolution factor with (a) faster, R_c = 0.32 °C/min, and (b) slower, R_c = 0.05 °C/min, cooling rates.

https://doi.org/10.1021/acs.oprd.1c00310
Org. Process Res. Dev. 2021, 25, 2551–2565

need to deal with a new chiral compound, the practitioner has to make difficult choices such as the initial asymmetry, the suspension density, the temperature levels, the temperature range, and so forth with only empirical criteria to follow.

The key novelty of this contribution is that it finally brings clarity how to make such choices and how to make them in a rational and optimal way, without the need for mathematical models and rigorous optimization.

We have reached this goal by first rescaling the model equations developed earlier[14] in such a way to simplify them to the point where the equations depend on a single dimensionless group defined through the process's operating conditions, that is, the dissolution factor, δ, representing the cycle capacity of the process, and a few system-dependent parameters, describing the temperature dependence of the system properties. Such structure of the rescaled mathematical model demonstrates that the dissolution factor controls the process performance; since it depends only on operating parameters (that the practitioner chooses and knows) and not on system parameters (that are difficult to measure and characterize, especially as a function of temperature), improving the process performance by tuning the value of the dissolution factor is simple and easy.

The extensive simulation and experimental study presented thereafter has demonstrated and rationalized the key role played by the initial dissolution factor, δ_0, as a design parameter in determining the performance of deracemization via periodic temperature cycles in terms of duration of the process and of productivity. Its primary effect on the number of cycles was found to be general for the various virtual systems analyzed, while the so called kinetic parameters of the model play only a secondary role. This conclusion was confirmed by a set of experimental results, some of which allowed to highlight and explain some peculiar dependencies on the system kinetics. Of particular interest is the high productivity achieved with low values of initial dissolution factor, when the corresponding initial enantiomeric excess and suspension density are suitably selected.

On one hand, these findings enable the identification of quasi-optimal operating conditions without the need for a rigorous mathematical process optimization and integrate the model-free design approach suggested in our previous work.[13] On the other hand, they serve as a basis to design and rationalize the implementation of non-periodic temperature cycles that were considered particularly promising in previous studies.[21] However, thanks to our process analysis based on the dissolution factor, which can be recalculated at every step of a non-periodic process, we have demonstrated (both in the lab and through simulations) that periodic temperature cycles outperform non-periodic temperature cycles, and we have rationalized and reinterpreted previous misleading results reported in the literature.[21]

Three final remarks, which also provide some perspective on future development, are worth noting. First, batch deracemization through periodic temperature cycles can be tuned and optimized by exploiting the combined effect of the different operating parameters grouped together in the initial dissolution factor, δ_0, and should be preferred to the same process implementing non-periodic cycles. Second, deracemization through periodic temperature cycles can also be implemented in a continuous mode, as presented earlier[39] and discussed in an upcoming publication.[23] Finally, the potential for productivity enhancement at low values of the initial dissolution factor, that is, at $\delta_0 = 0$, with an initial suspension consisting of an enantiopure solid in a racemic solution, that is, with $ee_0 = 1$, is going to be explored in a second upcoming publication;[28] this would be a simple batch cooling crystallization process with racemization in solution, which promises to exhibit attractive advantages but also a few disadvantages, with respect to the temperature cycles studied here.

AUTHOR INFORMATION

Corresponding Author

Marco Mazzotti − *Institute of Energy and Process Engineering, ETH Zurich, 8092 Zurich, Switzerland;* orcid.org/0000-0002-4948-6705; Phone: +41 44 632 24 56; Email: marco.mazzotti@ipe.mavt.ethz.ch; Fax: +41 44 632 11 41

Authors

Francesca Breveglieri − *Institute of Energy and Process Engineering, ETH Zurich, 8092 Zurich, Switzerland;* orcid.org/0000-0002-0034-7966

Brigitta Bodák − *Institute of Energy and Process Engineering, ETH Zurich, 8092 Zurich, Switzerland;* orcid.org/0000-0002-1979-9815

Complete contact information is available at: https://pubs.acs.org/10.1021/acs.oprd.1c00310

Notes

The authors declare no competing financial interest.

ACKNOWLEDGMENTS

This research received funding as part of the CORE Project (October 2016 to December 2020) from the European Union's Horizon 2020 Research and Innovation Program under Marie Sklodowska-Curie Grant Agreement 722456 CORE ITN and also from the European Research Council (ERC) under the European Unions Horizon 2020 Research and Innovation Programme under Grant Agreement no. 788607.

REFERENCES

(1) Jacques, J.; Collet, A. *Enantiomers, Racemates, and Resolutions*; John Wiley & Sons, Inc.: Hoboken, NJ, USA, 1981.

(2) Agranat, I.; Caner, H.; Caldwell, J. Putting chirality to work: the strategy of chiral switches. *Nat. Rev. Drug Discovery* **2002**, *1*, 753−768.

(3) Calcaterra, A.; D'Acquarica, I. The market of chiral drugs: Chiral switches versus de novo enantiomerically pure compounds. *J. Pharm. Biomed. Anal.* **2018**, *147*, 323−340.

(4) Lorenz, H.; Seidel-Morgenstern, A. Processes To Separate Enantiomers. *Angew. Chem., Int. Ed.* **2014**, *53*, 1218−1250.

(5) Lorenz, H.; Capla, F.; Polenske, D.; Elsner, M. P.; Seidel-Morgenstern, A. Crystallization Based Separation of Enantiomers * (Review). *J. Univ. Chem. Technol. Metall.* **2007**, *42*, 5−16.

(6) Intaraboonrod, K.; Lerdwiriyanupap, T.; Hoquante, M.; Coquerel, G.; Flood, A. E. Temperature cycle induced deracemization. *Mendeleev Commun.* **2020**, *30*, 395−405.

(7) Iggland, M.; Mazzotti, M. A Population Balance Model for Chiral Resolution via Viedma Ripening. *Cryst. Growth Des.* **2011**, *11*, 4611−4622.

(8) Noorduin, W. L.; Meekes, H.; van Enckevort, W. J. P.; Millemaggi, A.; Leeman, M.; Kaptein, B.; Kellogg, R. M.; Vlieg, E. Complete deracemization by attrition-enhanced Ostwald ripening elucidated. *Angew. Chem., Int. Ed.* **2008**, *47*, 6445−6447.

(9) Noorduin, W. L.; Izumi, T.; Millemaggi, A.; Leeman, M.; Meekes, H.; Van Enckevort, W. J. P.; Kellogg, R. M.; Kaptein, B.;

Vlieg, E.; Blackmond, D. G. Emergence of a single solid chiral state from a nearly racemic amino acid derivative. *J. Am. Chem. Soc.* **2008**, *130*, 1158−1159.
(10) Viedma, C. Chiral Symmetry Breaking During Crystallization: Complete Chiral Purity Induced by Nonlinear Autocatalysis and Recycling. *Phys. Rev. Lett.* **2005**, *94*, 065504.
(11) Suwannasang, K.; Flood, A. E.; Rougeot, C.; Coquerel, G. Using Programmed Heating−Cooling Cycles with Racemization in Solution for Complete Symmetry Breaking of a Conglomerate Forming System. *Cryst. Growth Des.* **2013**, *13*, 3498−3504.
(12) Breveglieri, F.; Maggioni, G. M.; Mazzotti, M. Deracemization of NMPA via Temperature Cycles. *Cryst. Growth Des.* **2018**, *18*, 1873−1881.
(13) Breveglieri, F.; Baglai, I.; Leeman, M.; Noorduin, W. L.; Kellogg, R. M.; Mazzotti, M. Performance Analysis and Model-Free Design of Deracemization via Temperature Cycles. *Org. Process Res. Dev.* **2020**, *24*, 1515−1522.
(14) Bodák, B.; Maggioni, G. M.; Mazzotti, M. Population-Based Mathematical Model of Solid-State Deracemization via Temperature Cycles. *Cryst. Growth Des.* **2018**, *18*, 7122−7131.
(15) Cameli, F.; Xiouras, C.; Stefanidis, G. D. Intensified deracemization via rapid microwave-assisted temperature cycling. *CrystEngComm* **2018**, *20*, 2897−2901.
(16) Li, W. W.; Spix, L.; de Reus, S. C. A.; Kramer, H. M.; Kramer, J. M.; Vlieg, E.; ter Horst, J. H. Deracemization of a Racemic Compound via Its Conglomerate-Forming Salt Using Temperature Cycling. *Cryst. Growth Des.* **2016**, *16*, 5563−5570.
(17) Oketani, R.; Hoquante, M.; Brandel, C.; Cardinael, P.; Coquerel, G. Practical Role of Racemization Rates in Deracemization Kinetics and Process Productivities. *Cryst. Growth Des.* **2018**, *18*, 6417−6420.
(18) Steendam, R. R. E.; ter Horst, J. H. Scaling Up Temperature Cycling-Induced Deracemization by Suppressing Nonstereoselective Processes. *Cryst. Growth Des.* **2018**, *18*, 3008−3015.
(19) Suwannasang, K.; Coquerel, G.; Rougeot, C.; Flood, A. E. Mathematical Modeling of Chiral Symmetry Breaking due to Differences in Crystal Growth Kinetics. *Chem. Eng. Technol.* **2014**, *37*, 1329−1339.
(20) Cameli, F.; ter Horst, J. H.; Steendam, R. R. E.; Xiouras, C.; Stefanidis, G. D. On the Effect of Secondary Nucleation on Deracemization through Temperature Cycles. *Chem.—Eur. J.* **2020**, *26*, 1344−1354.
(21) Suwannasang, K.; Flood, A. E.; Rougeot, C.; Coquerel, G. Use of Programmed Damped Temperature Cycles for the Deracemization of a Racemic Suspension of a Conglomerate Forming System. *Org. Process Res. Dev.* **2017**, *21*, 623−630.
(22) LeVeque, R. J. *Finite Volume Methods for Hyperbolic Problems*; Cambridge University Press: Cambridge, 2002.
(23) Bodák, B.; Mazzotti, M. Solid-State Deracemization via Temperature Cycles in Continuous Operation: A Model-based Process Design. in preparation.
(24) Breveglieri, F.; Mazzotti, M. Role of Racemization Kinetics in the Deracemization Process via Temperature Cycles. *Cryst. Growth Des.* **2019**, *19*, 3551−3558.
(25) Bodák, B.; Maggioni, G. M.; Mazzotti, M. Effect of Initial Conditions on Solid-State Deracemization via Temperature Cycles: A Model-Based Study. *Cryst. Growth Des.* **2019**, *19*, 6552−6559.
(26) Oketani, R.; Hoquante, M.; Brandel, C.; Cardinael, P.; Coquerel, G. Resolution of an Atropisomeric Naphthamide by Second-Order Asymmetric Transformation: A Highly Productive Technique. *Org. Process Res. Dev.* **2019**, *23*, 1197−1203.
(27) Levilain, G.; Rougeot, C.; Guillen, F.; Plaquevent, J.-C.; Coquerel, G. Attrition-enhanced preferential crystallization combined with racemization leading to redissolution of the antipode nuclei. *Tetrahedron: Asymmetry* **2009**, *20*, 2769−2771.
(28) Bodák, B.; Breveglieri, F.; Mazzotti, M. Modeling and experimental analysis of deracemization by cooling. in preparation.
(29) Noorduin, W. L.; Meekes, H.; van Enckevort, W. J. P.; Kaptein, B.; Kellogg, R. M.; Vlieg, E. Enantioselective Symmetry Breaking Directed by the Order of Process Steps. *Angew. Chem., Int. Ed.* **2010**, *49*, 2539−2541.
(30) van der Meijden, M. W.; Leeman, M.; Gelens, E.; Noorduin, W. L.; Meekes, H.; van Enckevort, W. J. P.; Kaptein, B.; Vlieg, E.; Kellogg, R. M. Attrition-Enhanced Deracemization in the Synthesis of Clopidogrel - A Practical Application of a New Discovery. *Org. Process Res. Dev.* **2009**, *13*, 1195−1198.
(31) Hein, J. E.; Huynh Cao, B.; Viedma, C.; Kellogg, R. M.; Blackmond, D. G. Pasteur's Tweezers Revisited: On the Mechanism of Attrition-Enhanced Deracemization and Resolution of Chiral Conglomerate Solids. *J. Am. Chem. Soc.* **2012**, *134*, 12629−12636.
(32) Noorduin, W. L.; van der Asdonk, P.; Bode, A. A. C.; Meekes, H.; van Enckevort, W. J. P.; Vlieg, E.; Kaptein, B.; van der Meijden, M. W.; Kellogg, R. M.; Deroover, G. Scaling Up Attrition-Enhanced Deracemization by Use of an Industrial Bead Mill in a Route to Clopidogrel (Plavix). *Org. Process Res. Dev.* **2010**, *14*, 908−911.
(33) Baglai, I.; Leeman, M.; Kaptein, B.; Kellogg, R. M.; Noorduin, W. L. A chiral switch: Balancing between equilibrium and non-equilibrium states. *Chem. Commun.* **2019**, *55*, 6910−6913.
(34) Iggland, M.; Fernández-Ronco, M. P.; Senn, R.; Kluge, J.; Mazzotti, M. Complete solid state deracemization by High Pressure Homogenization. *Chem. Eng. Sci.* **2014**, *111*, 106−111.
(35) Baglai, I.; Leeman, M.; Wurst, K.; Kaptein, B.; Kellogg, R. M.; Noorduin, W. L. The Strecker reaction coupled to Viedma ripening: a simple route to highly hindered enantiomerically pure amino acids. *Chem. Commun.* **2018**, *54*, 10832−10834.
(36) Maggioni, G. M.; Bosetti, L.; Dos Santos, E.; Mazzotti, M. Statistical analysis of series of detection time measurements for the estimation of nucleation rates. *Cryst. Growth Des.* **2017**, *17*, 5488−5498.
(37) Noorduin, W. L.; Meekes, H.; Bode, A. A. C.; van Enckevort, W. J. P.; Kaptein, B.; Kellogg, R. M.; Vlieg, E. Explanation for the Emergence of a Single Chiral Solid State during Attrition-Enhanced Ostwald Ripening: Survival of the Fittest. *Cryst. Growth Des.* **2008**, *8*, 1675−1681.
(38) Iggland, M.; Müller, R.; Mazzotti, M. On the Effect of Initial Conditions in Viedma Ripening. *Cryst. Growth Des.* **2014**, *14*, 2488−2493.
(39) Bodák, B.; Breveglieri, F.; Mazzotti, M. Continuous solid-state deracemization via temperature cycles: a model-based process development. *2020 Virtual AIChE Annual Meeting Conference Present*, 2020.

https://doi.org/10.1021/acs.oprd.1c00310
Org. Process Res. Dev. 2021, 25, 2551−2565